



Study on the Effect of Sandstone Microscopic Damage and Dynamic Compressive Properties After Heat Treatment

Fandong Meng¹ · Yubai Li¹ · Yue Zhai¹ · Yan Li¹ · Ruifeng Zhao¹ · Yunsheng Zhang¹

Received: 20 May 2021 / Accepted: 3 December 2021 / Published online: 22 January 2022
© The Author(s), under exclusive licence to Springer-Verlag GmbH Austria, part of Springer Nature 2021

Abstract

It has important guiding significance to study the influence of high temperature on physical and chemical properties and dynamic compression mechanical properties of rocks on the stability of rock mass engineering involving thermal behavior. The damage characteristics and dynamic mechanical characteristics of sandstone after different temperatures (20 °C, 200 °C, 400 °C, 600 °C, 800 °C, 1000 °C) are studied. The mineral composition, mineral content and pore structure of sandstone changed significantly after heat treatment. The content of clay minerals decreases and the content of quartz increases. And all the internal hematite is reduced at 400 °C. The content of macropores increases, and the pore size range decreases. The Split Hopkinson pressure bar is used to perform uniaxial impact compression tests on the heat-treated sandstone specimens with different average impact speeds (8.6 m/s, 14.6 m/s and 18.8 m/s). It is found that the impact speed would weaken the degrading effect of temperature on sandstone, and the temperature would increase the strengthening effect of strain rate. The change of the dynamic elastic modulus of sandstone under the coupling effect of temperature and loading includes the temperature weakening stage, the impact load enhancing stage and the temperature weakening stage. A damage dynamic constitutive model considering the combined effects of temperature initial damage and impact loading damage is established according to the study of the macroscopic and mesoscopic degradation characteristics of sandstone by temperature. The rationality of the model is verified.

Keywords Thermal damage · Pore structure · Dynamic mechanical properties · Constitutive model · X-ray diffraction · Sandstone

1 Introduction

The extraction of oil and natural gas (Castanier and Brigham 2003; Wang et al. 2018), underground nuclear waste storage (Zuo et al. 2010) and the extraction of thermal energy (Róañski et al. 2021) are all affected by the thermal behavior of rocks (Liu and Xu 2013). Heated minerals would expand and undergo a series of chemical reactions, resulting in changes in the physical and chemical properties of heat-treated rocks, such as the number of pores (Tao et al. 2020), mineral composition and structure (Hajpál and Török 2004). The cracks are extended due to the thermal stress generated by the high temperature, which leads to a decrease in the mechanical properties of the rock (Mahanta et al. 2016).

The risk of external fires and gas explosions increases as the mining depth increases (Li et al. 2018). The rock mass in underground engineering is inevitably disturbed by dynamic compression (Xie et al. 2020), which would affect the stability of the surrounding rock. Therefore, it is of great significance to the stability of rock mass engineering to study the influence of the physical and chemical properties of heat-treated rock on its dynamic performance.

Previous studies have found that the thermal expansion properties of rocks are affected by mineral composition, thermal expansion coefficient of minerals (Rijaniaina et al. 2016), initial porosity (Sippel et al. 2007) and grain size (Janio de Castro Lima and Paraguassú 2004). The permeability (Morrow et al. 1981) and porosity (Fan et al. 2018; Sirdesai et al. 2019) of the rock increase with increasing temperature. The elastic modulus (Tian et al. 2018), compressive strength (Zhao and Zhihong 2016), tensile strength (Guha Roy and Singh 2016), fracture toughness (Peng et al. 2020) and wave velocity are all reduced, and the anisotropy

✉ Yue Zhai
zy@chd.edu.cn

¹ School of Geology Engineering and Geomatics, Chang'an University, Xi'an 710064, China

of wave velocity is more obvious. And the mechanical properties of the rock are affected by the heating rate, cooling method (Kumari et al. 2017; Shen et al. 2020) and cooling rate (Shao et al. 2014; Zhang et al. 2020). The mechanical tests of heat-treated rocks are mostly static tests. The dynamic behavior of the rock mass cannot be ignored either (Fan et al. 2017; Li 2013; Li et al. 2015a, b, 2019; Yu et al. 2021). The dynamic compressive strength and tensile strength of heat-treated rock will decrease (Fan et al. 2020, 2017; Xu et al. 2021). The temperature-induced degradation of dynamic strength is not the same as static strength because it involves the effect of strain rate, and is more complicated.

In terms of damage constitutive models, the physical parameters (porosity, wave velocity, elastic modulus, CT number, thermal conductivity, density, and volume) that change after high temperature are used by most scholars to establish damage factors (Li et al. 2021). Then the stress–strain relationship is obtained using the theory of elasticity. But the influence of strain rate is not considered in this method. In the study of dynamic mechanics, it is generally considered that rock strength obeys a certain distribution, among which the Weibull distribution is recognized (Wang et al. 2007). Scholars established the dynamic loading damage factor based on this specific distribution form, and the dynamic stress–strain relationship is obtained. However, the initial damage of the rock is not considered in this method.

In this paper, Nuclear Magnetic Resonance (NMR), Magnetic Resonance Imaging (MRI) and X-ray diffraction (XRD) tests are used to analyze the meso-scale physical and chemical properties of sandstone after heat treatment. The $\Phi 100$ mm Split Hopkinson pressure bar (SHPB) is used to research the dynamic compressive performance of sandstone specimens after heat treatment. The relationship between the change characteristics of pores and cracks and the macroscopic dynamic compressive characteristics of the sandstone after heat treatment is discussed, and a constitutive model considering the temperature damage and the dynamic loading damage is established and verified.

2 Experimental Procedure

2.1 Sandstone Preparation

The sandstone specimens used in this paper were taken from northern Shaanxi, China. The area is rich in mineral resources, dominated by rocky landforms. The specimen was processed into a cylinder with a diameter of 98 mm and a height of 50 mm for subsequent tests. The accuracy of the specimens meets the requirements of “Engineering Rock Mass Test Method Standard” (GB/T50266-2013) and

“International Society for Rock Mechanics” (ISRM). The error of the height and diameter of the specimens shall not be greater than ± 0.3 mm, the error of parallelism shall be less than ± 0.05 mm, and the non-perpendicularity of the surface shall be less than $\pm 0.25^\circ$.

2.2 Test Process

The selected sandstone specimens were prepared for the following tests:

- a. Thermal treatment. Temperature control equipment (model: AI-518) and muffle furnace (model: SX2-10-13) were used as heating test instruments in this paper. The maximum heating temperature of the instrument is 1300°C , and the temperature control accuracy is 1°C . Six different temperatures (room temperature 20°C , 200°C , 400°C , 600°C , 800°C , 1000°C) were set in the heating test. The heating curve is shown in the Fig. 1. The temperature was kept constant for 2 h after reaching the target temperature, it is considered that the temperature of the inner and outer surfaces of specimen is consistent (see Fig. 2).
- b. NMR test. The NMR phenomenon refers to the relaxation behavior of the spin hydrogen nuclei in the fluid contained in the rock in a constant magnetic field and a radio frequency magnetic field (Li et al. 2020). NMR test of saturated sandstone specimens can indirectly obtain the internal pore structure. The vacuum pumping equipment was filled with distilled water exceeding the specimen. The vacuum pumping equipment was continuously pumped for 4 h at a pressure of 0.1 MPa until no bubbles overflow on the surface of the specimens, and then soaked for more than 24 h to obtain a water-saturated specimen. The saturated specimens were put into the low-field NMR system (model: MacroMR12-150H-I). The change of the pores inside the sandstone specimen after heat treatment was analyzed.
- c. XRD test. D/max 2500 X-ray powder crystal diffractometer (Fig. 3) was used. The heat-treated specimens were ground and then subjected to XRD test to analyze the change of mineral composition with temperature.
- d. SHPB test. The $\Phi 100$ mm SHPB system was used to study the dynamic mechanical properties of sandstone specimens after heat treatment under different impact speeds. The material of the pressure bars is 45Cr alloy steel, the density is 7850 kg/m^3 , and the elastic modulus is 210 GPa. The length of the incident bar is 4400 mm, and the length of the transmission bar is 3000 mm. The stress pulse signals are collected through the two strain gauges on the incident bar and the transmission bar. The collected pulse signals are converted and amplified by the super dynamic strain gauge, and then stored by the

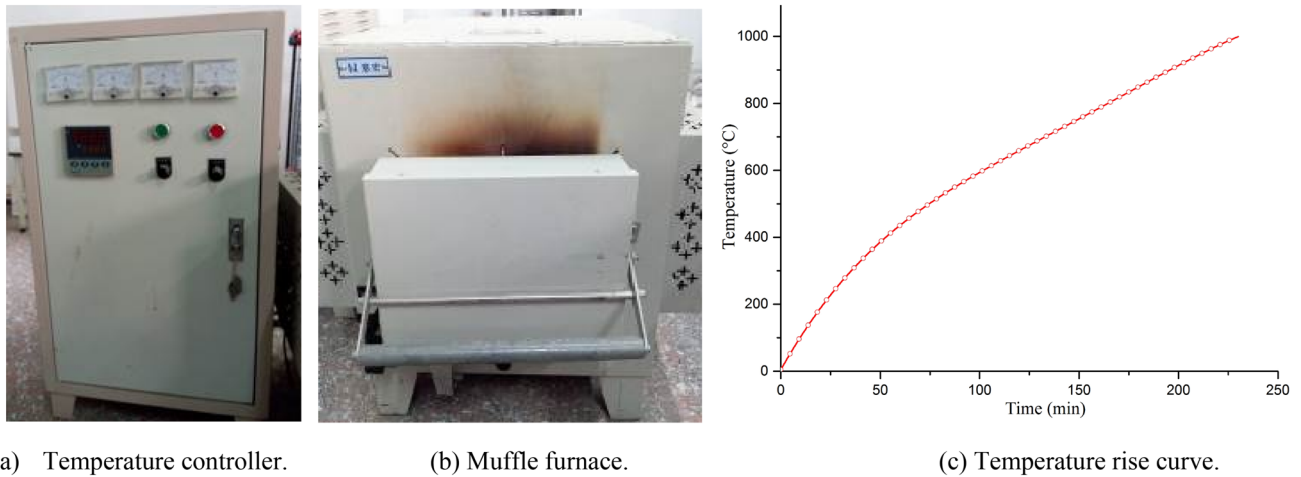
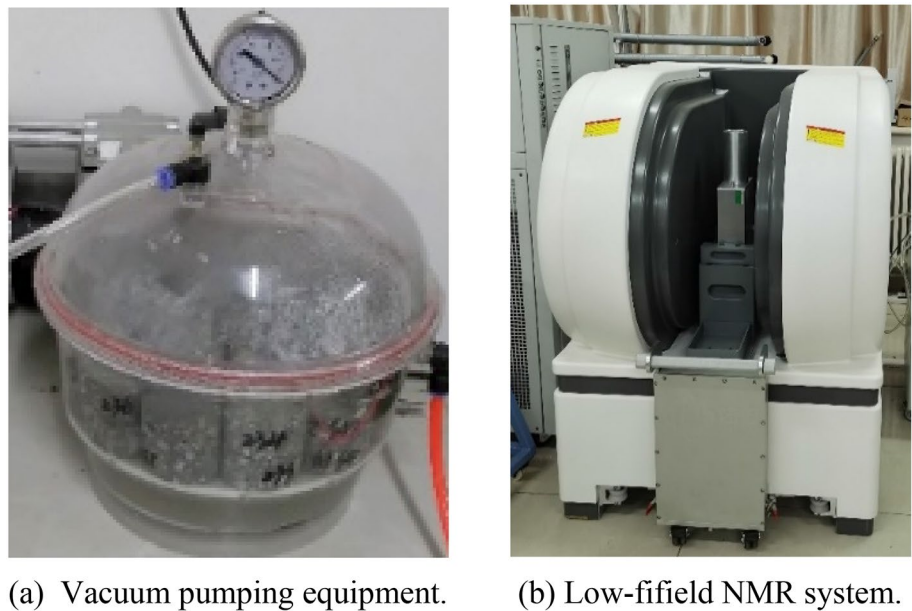


Fig. 1 Heating test

Fig. 2 NMR Test



computer. In the SHPB test, three types of impact air pressure (0.2 MPa, 0.35 MPa, 0.5 MPa) were set, and the impact compression test was performed on the specimens treated at six temperatures. The average impact speeds corresponding to the three impact air pressures were 8.6 m/s, 14.6 m/s and 18.8 m/s, respectively. Three specimens were designed for each working condition, so there were a total of 54 sandstone specimens in this test (see Fig. 4).

3 Microstructure of Sandstone After Heat Treatment

3.1 Mineral Composition of Heat-Treated Sandstone

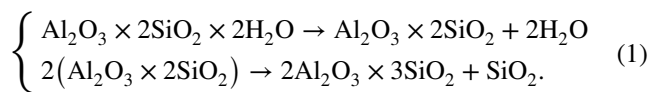
It can be found the surface color of the sandstone specimen becomes red obviously after the heat treatment from Fig. 5. And visible cracks appeared on the surface of the specimens.



Fig. 3 X-ray powder diffractometer

The mineral diffraction patterns (Fig. 6) and composition content changes (Fig. 7) of the sandstone specimens after heat treatment at different temperatures are obtained through the XRD test. The sandstone specimens used contains 93.1% quartz at room temperature, indicating that this type of sandstone belongs to quartz sandstone. It also contains a small amount of clay minerals and hematite in addition to a large amount of quartz. The content of clay

minerals and hematite decreased, and the content of quartz increased after the action of high temperature. Hematite is reduced to Fe after high temperature. It can be found from Fig. 7 that all hematite is reduced to Fe at 400 °C. Under the action of high temperature, some clay minerals decompose to produce red minerals. The above two reasons cause the surface of the sandstone to be dark red after heat treatment at 400 °C. The texture of the sandstone surface is clearer. Kaolinite is taken as an example among clay minerals. Kaolinite ($\text{Al}_2\text{O}_3 \cdot 2\text{SiO}_2 \cdot 2\text{H}_2\text{O}$) undergoes dehydroxylation (Zhang et al. 2019) between 500 and 600 °C. As the temperature rises, the kaolinite undergoes a phase change, and the SiO_2 phase is precipitated. This is the reason why the total amount of clay minerals has decreased and the quartz content has increased.



3.2 Pore Characteristics of Heat-Treated Sandstone

3.2.1 Porosity Variation Analyses

After the NMR test, the porosity of the heat-treated sandstone is obtained. The relationship between porosity and temperature is analyzed. It can be found from Fig. 8 that the porosity of the sandstone specimens increases with the increase of temperature, and the overall rise in an "S" shape. Between 20 and 400 °C, the porosity gradually increases as the temperature increases. When the temperature is greater than 400 °C, the rate of increase drops. The fitting curve is obtained by fitting the scattered

Fig. 4 Split Hopkinson pressure bars (SHPB) equipment

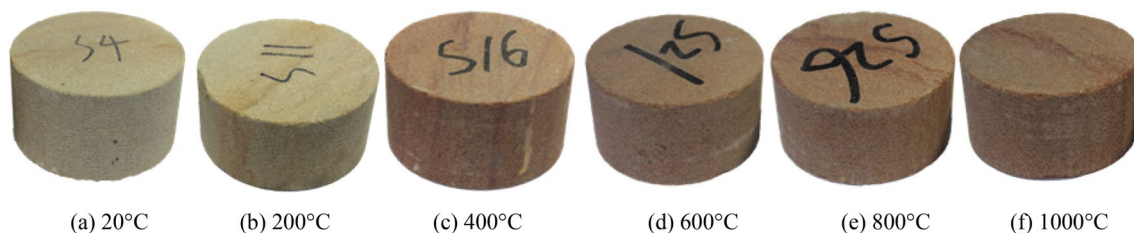


Fig. 5 The apparent morphology of heat-treated sandstone specimens

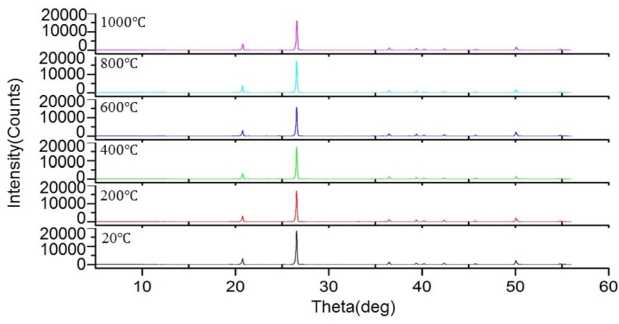


Fig. 6 X-ray diffraction data of heat-treated sandstone

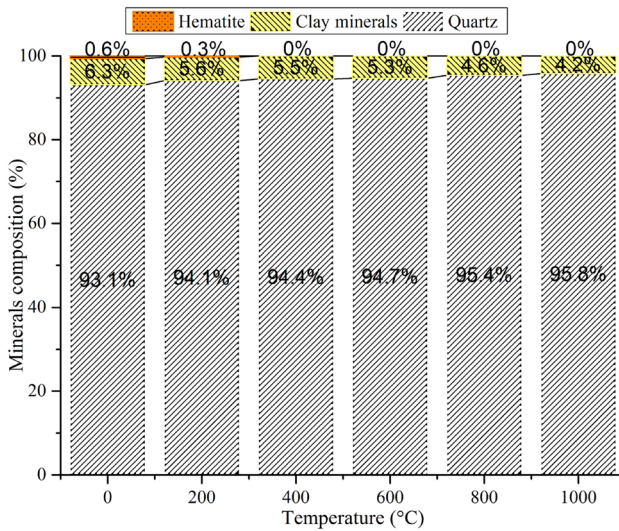


Fig. 7 Changes in mineral content

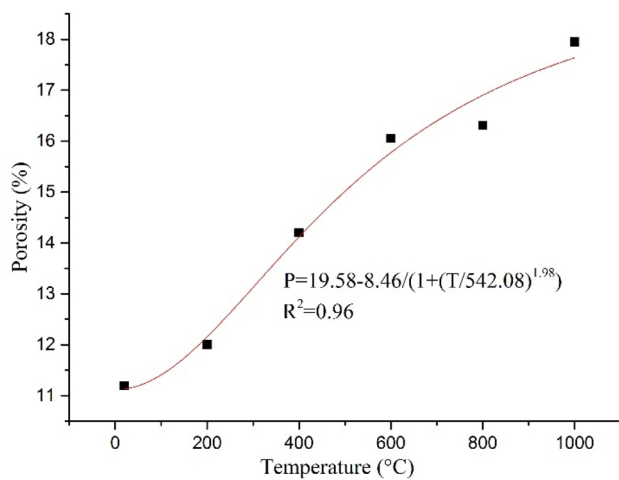


Fig. 8 Variation of porosity with temperature

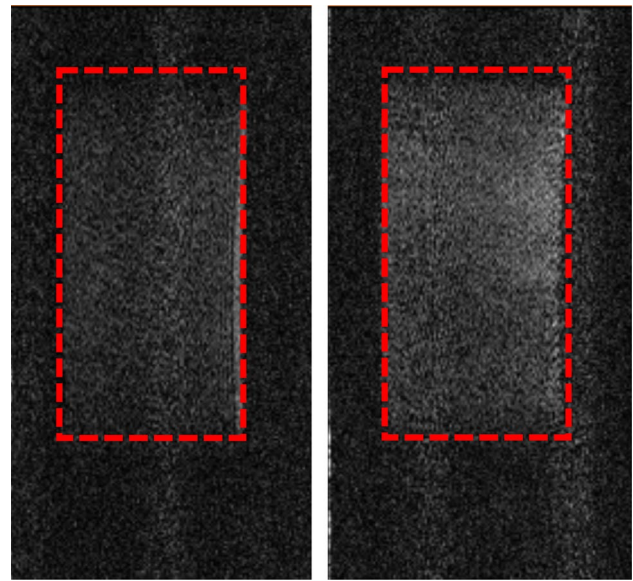


Fig. 9 MRI of heat-treated sandstone

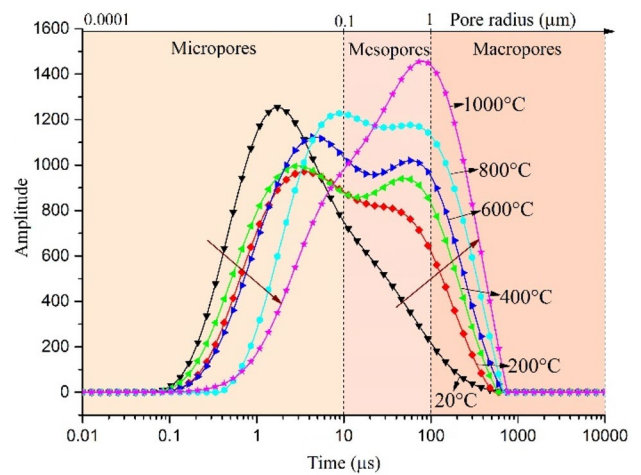


Fig. 10 Variation of T₂ spectrum

points, and the fitting effect is good. The second derivative of the porosity-temperature relationship is calculated, and the temperature corresponding to the inflection point is determined to be 311 °C. In other words, the porosity of the sandstone specimen increases the most when the temperature is 311 °C.

The two-dimensional grayscale image obtained by MRI test is shown in Fig. 9. Based on the introduction in Sect. 3.1, iron is reduced at 400 °C. Specimens containing metallic minerals could affect MRI imaging. So, only 20 °C and 200 °C are shown here. It can be found that the pores increase significantly at 200 °C.

3.2.2 T₂ Spectrum Analysis

The T₂ spectrum of the heat-treated sandstone specimen is obtained by the NMR test, as shown in the Fig. 10. The transverse relaxation time has a linear relationship with the pore radius:

$$r = C \times T_2, \tag{2}$$

where r is the pore radius. C is the conversion coefficient. $C = F_S \times \rho$. F_S is the geometry factor (for the spherical pores $F_S = 3$; and for the columnar pores $F_S = 2$). ρ is crosswise surface relaxation strength ($\mu\text{m}/\text{ms}$). The value of C is regionally empirical. In China, the value of C is generally 0.01–0.15 $\mu\text{m}/\text{ms}$ for most sandstones(Li et al. 2006). In this paper, the value of C is 0.01 for the convenience of research.

According to the existing research results (Meng et al. 2021), the pores inside the specimens are determined as macropores ($\geq 1 \mu\text{m}$), mesopores (0.1–1 μm) and micropores ($< 0.1 \mu\text{m}$) according to the pore radius. According to the relationship of Eq. (2), the cumulative percentage distribution of the pore radius of the sandstone specimens after heat treatment at different temperatures is obtained (Fig. 11). It can be found that each curve in the T₂ spectrum has approximately two peaks. As the temperature increases, the curve tends to move to the right. The left peak gradually decreases, and the right peak gradually increases. That is to

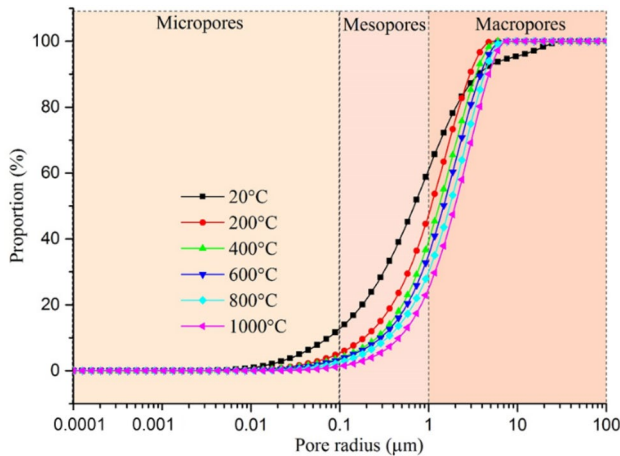
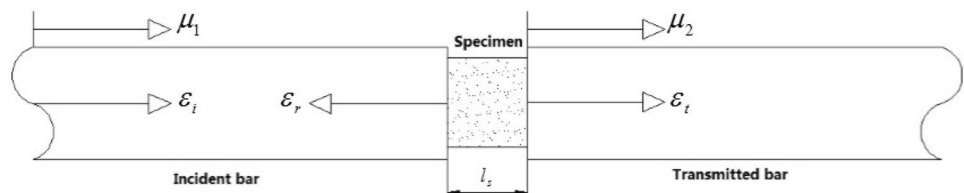


Fig. 11 Cumulative percentage distribution of pore size

Fig. 12 Schematic diagram of calculation



say, the content of macropores inside the specimen gradually increases as the temperature increases. This is also reflected in Fig. 11. As the temperature increases, the curve moves to the right. It shows that the lower the temperature acting on the sandstone specimen, the larger the pore size range of the specimen, the pores of various sizes are included. It is verified that the effect of high temperature would enlarge the pore size inside the sandstone specimens.

4 Analysis of SHPB Test Results

4.1 Test Principle

It is assumed that the equipment and specimens during the SHPB test are isotropic and satisfy the one-dimensional stress wave theory. The calculation principle diagram is shown in Fig. 12.

The average stress σ , strain rate $\dot{\epsilon}$ and strain ϵ of the sandstone specimen are calculated by Eqs. (3)–(5) (Gong et al. 2019; Li et al. 2017):

$$\dot{\epsilon} = -\frac{\mu_1 - \mu_2}{l_s} = \frac{C_0}{l_s} (-\epsilon_i + \epsilon_r + \epsilon_t), \tag{3}$$

$$\epsilon = \frac{C_0}{l_s} \int_0^t (-\epsilon_i + \epsilon_r + \epsilon_t) d\tau, \tag{4}$$

$$\sigma = \frac{E_0 A}{2A_s} (\epsilon_i + \epsilon_r + \epsilon_t), \tag{5}$$

where C_0 , A and E_0 are the wave velocity, cross-sectional area and elastic modulus of the bar, respectively. A_s and l_s are the cross-sectional area and height of the sandstone specimen, respectively. ϵ_i is the incident strain. ϵ_t is the transmission strain, and ϵ_r is the reflection strain.

4.2 Dynamic Stress Equilibrium

During the SHPB test, it is an effective dynamic compression test that the specimen is in a state of stress equilibrium before it is broken (Zhou et al. 2017). It is considered that the specimen is in a state of stress equilibrium if the following Eq. (6) is satisfied (Chen et al. 2018). The stress

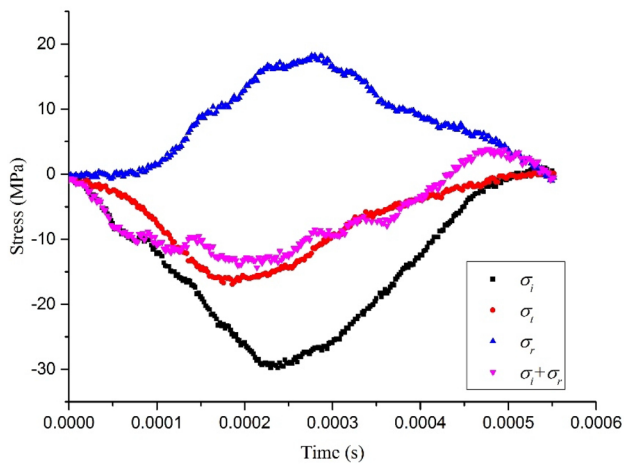


Fig. 13 Dynamic stress equilibrium verification

state when the average impact speed reaches 18.8 m/s is shown in Fig. 13. It can be found that the sum of the incident stress and the reflected stress almost coincides with the

transmission stress curve, which means that the specimen is in a state of stress equilibrium during the dynamic loading process.

$$\sigma_t = \sigma_i + \sigma_r, \tag{6}$$

where σ_i is the incident stress, σ_r is the reflected stress and σ_t is the transmission stress.

4.3 Stress–Strain Curve Characteristics

According to Eqs. (3)–(5), the stress and strain of sandstone specimens at each time can be calculated. The stress–strain curve of sandstone after heat treatment is obtained (Fig. 14). It can be found from Fig. 14 that the curve includes three stages of the conventional stress–strain curve (Li et al. 2020): the elastic deformation stage, the plastic deformation stage and the failure stage. There is no obvious pore compaction stage. This may be because the rock crystals have no enough time to close due to the large inertia during the impact. It can be indicated

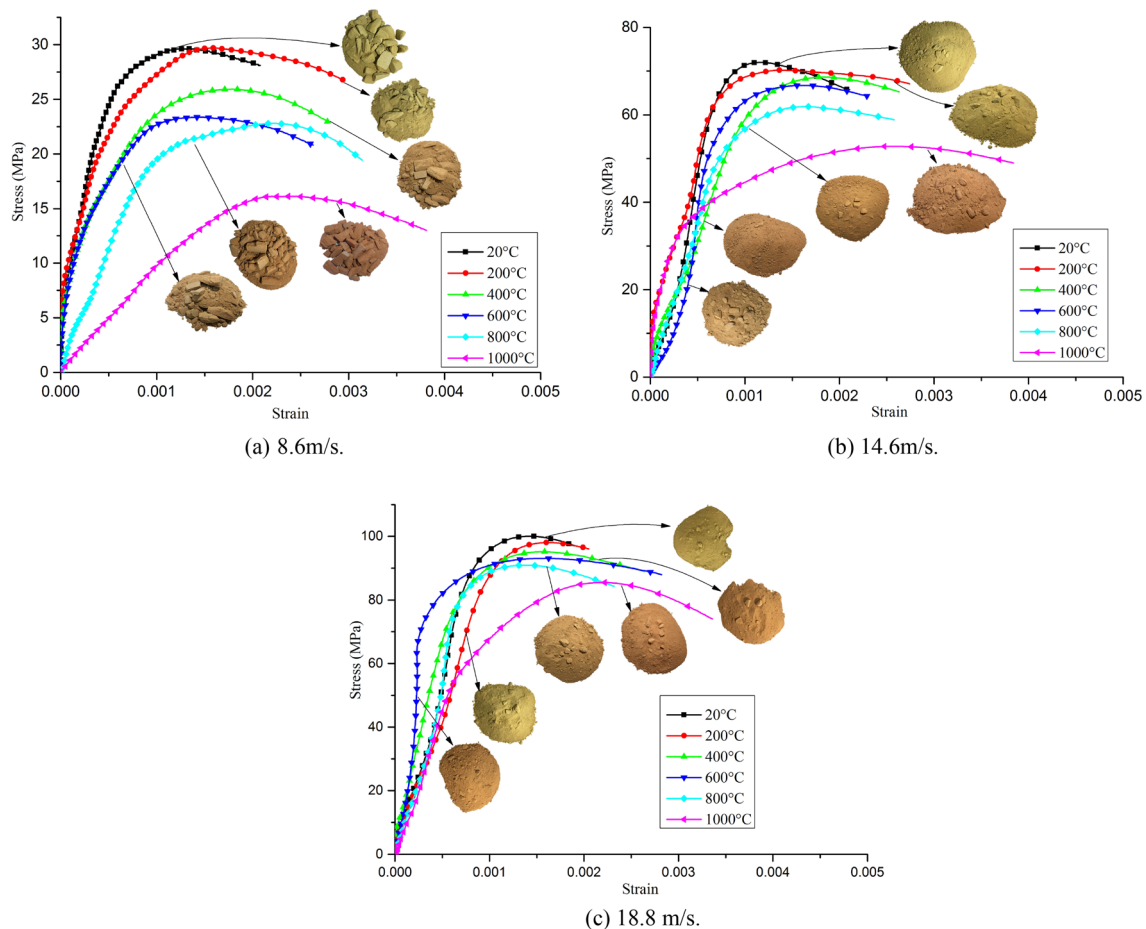


Fig. 14 Stress–strain curve of sandstone after heat treatment

that the high temperature damage to the sandstone specimen would directly lead to the decrease of the dynamic compressive strength. As the temperature increases, the dynamic peak stress of sandstone decreases significantly, which is more obvious during low-speed impact. When the average impact speed increases, the strain rate of the specimen must be increased, so that the dynamic peak strength increases. Therefore, when the average impact speed is 8.6 m/s, the peak strength at 1000 °C is reduced by 45.53% compared to that at 20 °C. When the average impact speed is 18.8 m/s, it is reduced by 14.55%. It can be seen from the Fig. 14 that the broken shape of sandstone becomes more broken with the increase of temperature and impact speed.

4.4 Deterioration of Temperature

As described in Sec. 4.3, the uniaxial dynamic compressive strength of sandstone specimens decreases with the increase of temperature under the same impact speed. There are many reasons why temperature deteriorates the mechanical properties of rocks. At 573 °C, quartz will undergo a transition from the triangular α phase to the hexagonal β phase (Barshad 1952). Clay minerals would also decompose in this temperature range as introduced in Sect. 3.1. In addition, the bound water of clay minerals breaks away between 100 and 450 °C (Jin et al. 2019; Wong et al. 2020). Mineral dehydration will shrink (Mahanta et al. 2016). This create cracks on the surface of the crystal grains. Fine-grained grains are more sensitive to temperature than coarse-grained grains (Malaga-Starzec et al. 2006). Various minerals undergo thermal expansion when subjected to high temperatures. Quartz has the largest thermal expansion coefficient compared to other rock-forming minerals (Wong et al. 2020). This series of physical and chemical reactions, such as phase change and decomposition due to high temperature, causes the crystal grains to shrink or expand and result in microcracks. The effect of high temperature would cause the microcracks inside the rock to propagate. Microcracks include two types according to their propagation mechanism during heating: thermally induced microcracks (Freire-Lista et al. 2016; Rathnaweera et al. 2018) and stress and thermally induced microcracks (Rao and Murthy 2001). The expansion of these two types of microcracks under the action of high temperature is also the main reason for the decrease of the dynamic compressive strength. It should be noted that during the microcrack propagation process pointed out by previous scholars in the research (Ranjith et al. 2012; Wong et al. 2020), the phenomenon of filling the original cracks to increase the strength is not reflected in the sandstone specimens.

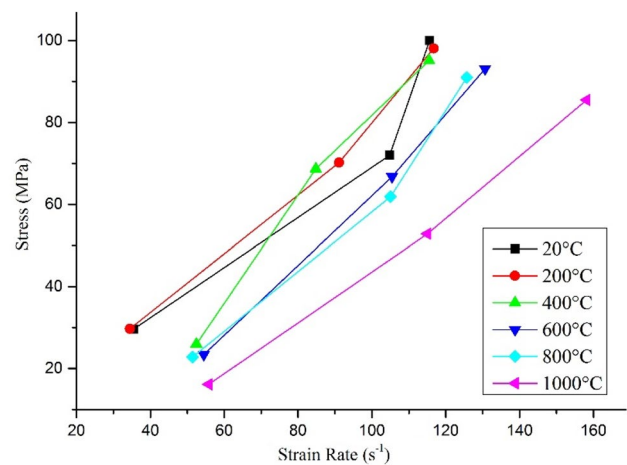


Fig. 15 Variation of stress with strain rate

4.5 Relationship Between Peak Stress and Strain Rate

Strain rate is a non-negligible part in the study of rock dynamic mechanical properties (Feng et al. 2021; Qi and Qian 2003). The relationship between uniaxial dynamic compressive strength, strain rate and heating temperature is shown in Fig. 15. It can be found that the dynamic peak strength of the sandstone specimen after the same temperature is increased with the increase of the strain rate. With the increase of the strain rate, the peak strength growth rate of the sandstone specimens at the six temperatures are: 20 °C: 237.94%, 200 °C: 230.24%, 400 °C: 267.02%, 600 °C: 298.43%, 800 °C: 298.86%, 1000 °C: 430.22%. The heat-treated sandstone specimens have obvious strain rate strengthening phenomenon is shown. And this phenomenon becomes more obvious as the temperature rises. This is because the internal damage of the rock becomes more serious as the temperature rises. The weaker the rock, the higher the sensitivity to strain rate (Feng et al. 1986). Therefore, the growth rate of the dynamic peak strength increases with the increase of temperature. It shows that temperature will strengthen the rate dependence of sandstone specimens.

4.6 Dynamic Elastic Modulus Analysis

The dynamic elastic modulus (E) of rock is not only related to the rock properties, but also to the loading rate (Grote et al. 2001; Sukontasukkul et al. 2004). E is obtained by calculating the slope of the elastic stage of the dynamic stress–strain curve (Zhou et al. 2017). The E -temperature relationship curve (Fig. 16) is drawn in order to discuss the E change law of heat-treated rock after impact load. It can be seen from Fig. 16 that the E of heat-treated sandstone generally shows a decreasing trend with the increase of temperature when

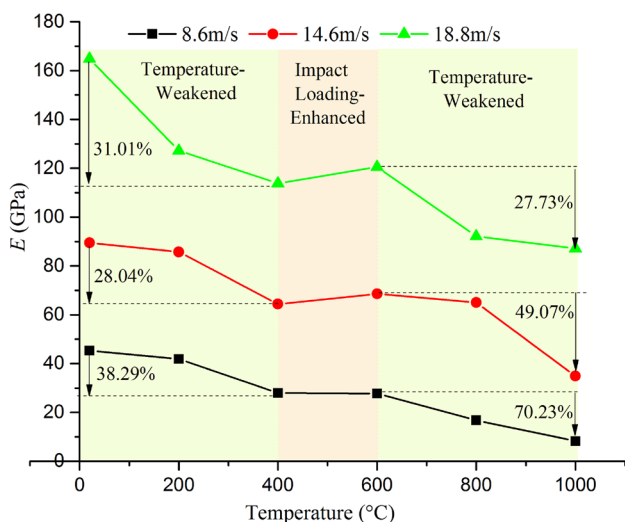


Fig. 16 Variation of E with temperature

the average impact speed is the same. E increases in a small range during 400–600 °C, this phenomenon occurs under the action of three average impact speeds. It is indicated that the enhancement effect of impact loading on the E is obvious in this temperature range. In other temperature ranges, the degradation effect of temperature on the E is stronger than the strengthening effect of impact loading. When the average impact speed is 8.6 m/s and 14.6 m/s, the decline rate of E at 600–1000 °C is significantly greater than that at 20–400 °C. This is the opposite when the average impact speed is 18.8 m/s. It shows that the effect of impact loading on the E is more obvious when the average impact speed is 18.8 m/s. It can also be clearly seen from Fig. 16 that the E of sandstone after the same temperature action increases significantly with the increase of the average impact speed. Because the strain rate increases under the action of high impact speed, which reduces the plastic deformation, the slope of the elastic deformation stage increases.

5 Dynamic Damage Constitutive Model of Heat-Treated Rock

5.1 Damage Constitutive Model Establishment

According to the principle of strain equivalence (Lemaitre 1984), the total damage variable D of the rock considering thermal damage after impact loading is:

$$D = D_0 + D_i - D_0D_i, \tag{7}$$

where D₀ is the thermal damage variable, D_i is the impact load damage variable.

The macropores in the specimen are more likely to cause damage to the rock than the micropores. Therefore, the initial damage factor D₀ established in the previous study considering the weight of the influence of the pore size on the strength of the specimen is used:

$$D_0 = \frac{w_1A'_{mic} + w_2A'_{mes} + w_3A'_{mac}}{w_1A_{mic} + w_2A_{mes} + w_3A_{mac}} - 1, \tag{8}$$

among them, w₁, w₂, and w₃ are the weights of micropores, mesopores and macropores on the damage of the rock. $w_i = \frac{V_i}{\sum V_i}$, V_i is the coefficient of variation of the corresponding pore content (Meng et al. 2021). A_{mic}, A_{mes} and A_{mac} are the area corresponding to micropores, mesopores and macropores in the T₂ spectrum of the sandstone at room temperature after the NMR test. A'_{mic}, A'_{mes} and A'_{mac} are the area corresponding to micropores, mesopores and macropores in the T₂ spectrum of the heat-treated sandstone after the NMR test.

The weights w₁, w₂, and w₃ of micropores, mesopores and macropores are calculated to be 0.232, 0.243 and 0.525, respectively. Then:

$$D_0 = \frac{0.232A'_{mic} + 0.243A'_{mes} + 0.525A'_{mac}}{0.232A_{mic} + 0.243A_{mes} + 0.525A_{mac}} - 1. \tag{9}$$

The strength of the rock obeys the Weibull statistical distribution (Cui et al. 2020; Wang et al. 2007), and the damage variable D_i:

$$D_i = \begin{cases} 1 - \exp \left[-\left(\frac{F_d}{F_0}\right)^m \right], & F_d \geq 0 \\ 0, & F_d < 0 \end{cases} \tag{10}$$

where m and F₀ are Weibull distribution parameters. F_d is the dynamic micro-element strength of the rock.

After uniaxial impact compression, the dynamic micro-element strength F_d of the rock is (Cao et al. 2017; Qi and Qian 2003):

$$F_d = E\varepsilon - k - \alpha \ln \frac{\dot{\varepsilon}}{\dot{\varepsilon}_0} - \frac{\beta \left(\frac{\dot{\varepsilon}}{\dot{\varepsilon}_s}\right)^n}{\left(\frac{\dot{\varepsilon}}{\dot{\varepsilon}_s}\right)^n + 1}, \tag{11}$$

where k = 2c cos φ / (1 - sin φ). c is the cohesion of the rock, φ is the angle of internal friction. α is a constant, ε̇₀ is the uniaxial ultimate strain rate of the rock. β is the maximum contribution of macroscopic viscosity to strength growth. ε̇_s is the strain rate corresponding to the inflection point of the semi-logarithmic curve of the rock material, and n is the material constant.

So, the total damage variable D is:

Table 1 c and φ of heat-treated sandstone (Ming and Ming 2017)

Parameter	20 °C	200 °C	400 °C	600 °C	800 °C	1000 °C
c	39.26	27.31	22.76	17.38	14.33	6.32
φ	23.17	16.74	14.49	11.94	10.66	6.87

$$D = \begin{cases} 1 - \left(2 - \frac{0.232A'_{mic} + 0.243A'_{mes} + 0.525A'_{mac}}{0.232A_{mic} + 0.243A_{mes} + 0.525A_{mac}} \right) \exp \left[- \left(\frac{F_d}{F_0} \right)^m \right], & F_d \geq 0 \\ \frac{0.232A'_{mic} + 0.243A'_{mes} + 0.525A'_{mac}}{0.232A_{mic} + 0.243A_{mes} + 0.525A_{mac}} - 1, & F_d < 0. \end{cases} \tag{12}$$

Based on the basic theory of continuous damage mechanics, the damage constitutive equation can be expressed as:

$$\sigma = E(1 - D)\epsilon. \tag{13}$$

Incorporating Eq. (12) into Eq. (13), the constitutive equation of heat-treated rock damage is obtained:

$$\sigma = \begin{cases} E \left(2 - \frac{0.232A'_{mic} + 0.243A'_{mes} + 0.525A'_{mac}}{0.232A_{mic} + 0.243A_{mes} + 0.525A_{mac}} \right) \exp \left[- \left(\frac{F_d}{F_0} \right)^m \right] \epsilon, & F_d \geq 0 \\ E \left(2 - \frac{0.232A'_{mic} + 0.243A'_{mes} + 0.525A'_{mac}}{0.232A_{mic} + 0.243A_{mes} + 0.525A_{mac}} \right) \epsilon, & F_d < 0. \end{cases} \tag{14}$$

(Eq. 18) proposed by Cao (Cao et al. 2017). The values of α , β and n (Tab. 2) are obtained by nonlinear fitting of experimental data and Eq. 18.

5.2 Parameter Solving and Model Verification

The values of c and φ refer to the research results of Ming and Ming (2017). The values of c and φ of sandstone after heat treatment at different temperatures are shown in Table 1.

According to the extreme value characteristics of the stress–strain curve, Eq. (14) satisfies the following two conditions:

$$\sigma(\epsilon_{max}) = \sigma_p \tag{15}$$

$$\left. \frac{\partial \sigma}{\partial \epsilon} \right|_{\epsilon = \epsilon_{max}} = 0, \tag{16}$$

where σ_p is the dynamic compressive peak stress, ϵ_{max} is the peak strain, at this time $F_d = F_{dp}$. F_0 and m are obtained.

$$F_0 = F_{dp} \ln \epsilon_{max} E_1 - D_0 \sigma_p - 1 \text{ mm} = F_{dp} F_0 E \epsilon_{max} \ln \epsilon_{max} E_1 - D_0 \sigma_p. \tag{17}$$

In addition to satisfying the relationship of Eq. 11, α , β and n also satisfy the nonlinear dynamic strength criterion

$$\sigma_p = k + \alpha \ln \frac{\dot{\epsilon}}{\dot{\epsilon}_0} + \frac{\beta \left(\frac{\dot{\epsilon}}{\dot{\epsilon}_s} \right)^n}{\left(\frac{\dot{\epsilon}}{\dot{\epsilon}_s} \right)^n + 1}. \tag{18}$$

The parameters are brought into Eq. 14, and the stress–strain relationship is obtained. The stress–strain curve of the specimen treated at 1000 °C under the average impact speed of 8.6 m/s is taken as an example, and the theoretical curve is compared with the test curve (Fig. 17). These two curves almost coincide. It is proved that the constitutive model based on the nonlinear dynamic strength criterion

Table 2 Dynamic strength parameters of heat-treated sandstone

Temperature/°C	α	β	n	$\dot{\epsilon}_s/s$	R^2
20	-4.68	105.02	11.74	106.53	0.99
200	-2.39	89.14	5.92	92.12	0.98
400	-3.23	112.24	3.84	79.24	0.99
600	-2.65	353.32	1.99	219.17	0.99
800	-0.61	97.25	7.01	110.55	0.98
1000	-0.53	181.09	2.53	173.72	0.99

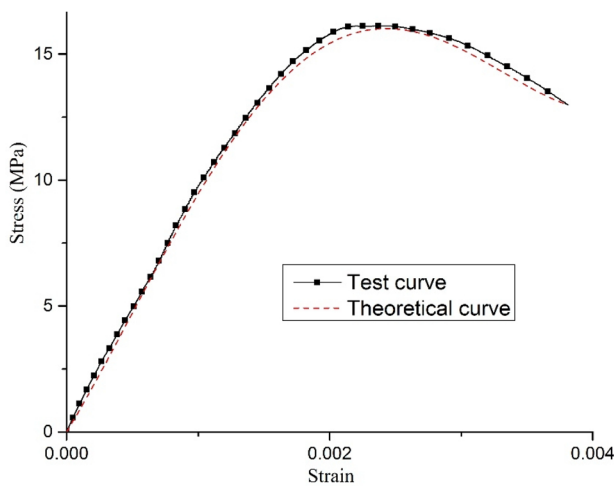


Fig. 17 Damage constitutive equation verification

considering the initial thermal damage and loading damage is reasonable and it can be well applied to the research of this paper.

6 Conclusions

The physicochemical properties and uniaxial dynamic compressive strength of sandstone after heat treatment are discussed in this paper. The research conclusions are as follows:

- (1) All the hematite in the sandstone is reduced when heat treated at 400 °C. After sandstone heat treatment, clay minerals are decomposed so that its content decreases and the quartz content increases. The surface of the specimen turns dark red. The content of large pores inside the sandstone is increased, and the pore size range is reduced due to the effect of high temperature. The relationship between porosity and temperature satisfies the characteristics of the S-shaped curve. The porosity growth rate reaches its maximum value at 311 °C, which is 0.95%.
- (2) The temperature degradation effect is more pronounced under the action of low impact speeds. Under the action of the average impact speed of 18.8 m/s, the decrease rate of peak stress caused by temperature is 3 times lower than that at 8.6 m/s. Temperature would strengthen the rate dependence of sandstone specimens. The growth rate of the peak stress with strain rate at 1000 °C is twice the growth rate of 20 °C.
- (3) The dynamic elastic modulus of heat-treated sandstone changes with the increase of temperature including three stages: decrease–increase–decrease. The three stages correspond to the temperature weakening zone,

the impact load enhancing zone and the temperature weakening zone.

- (4) The dynamic damage constitutive model of heat-treated rock is established by considering thermal damage and impact loading damage, the theoretical curve obtained is very close to the experimental curve. It has been verified that the proposed model is reasonable.

Acknowledgements The authors would like to acknowledge financial supports by the National Natural Science Foundation of China (No. 41941019 and 41772277), department of science and technology of Shaanxi Province (No. 2021TD-55), “111” Center, program of the Ministry of Education of China (No. B18046), and the Fundamental Research Funds for the Central Universities, CHD (No. 300102261101).

References

- Barshad I (1952) Temperature and heat of reaction calibration of the differential thermal analysis apparatus. *Am Mineral* 37:667–694
- Cao W, Lin X, Zhang C, Yang S (2017) A statistical damage simulation method of dynamic deformation process for rocks based on nonlinear dynamic strength criterion. *Chin J Rock Mech Eng* 36:794–802
- Castanier LM, Brigham WE (2003) Upgrading of crude oil via in situ combustion. *J Petrol Sci Eng* 39:125–136
- Chen R, Yao W, Lu F, Xia K (2018) Evaluation of the stress equilibrium condition in axially constrained triaxial SHPB tests. *Exp Mech* 58:527–531. <https://doi.org/10.1007/s11340-017-0344-5>
- Cui T, He H, Yan W, Zhou D (2020) Compression damage constitutive model of hybrid fiber reinforced concrete and its experimental verification. *Constr Build Mater* 264:120026. <https://doi.org/10.1016/j.conbuildmat.2020.120026>
- Fan LF, Wu ZJ, Wan Z, Gao JW (2017) Experimental investigation of thermal effects on dynamic behavior of granite. *Appl Therm Eng* 125:94–103. <https://doi.org/10.1016/j.applthermaleng.2017.07.007>
- Fan LF, Gao JW, Wu ZJ, Yang SQ, Ma GW (2018) An investigation of thermal effects on micro-properties of granite by X-ray CT technique. *Appl Therm Eng* 140:505–519. <https://doi.org/10.1016/j.applthermaleng.2018.05.074>
- Fan L, Gao J, Du X, Wu Z (2020) Spatial gradient distributions of thermal shock-induced damage to granite. *J Rock Mech Geotech Eng* 12:917–926. <https://doi.org/10.1016/j.jrmge.2020.05.004>
- Feng Y, Qiu Y, Li Z (1986) The Effect of Strain Rate on Strength and Deformability of Rock. *Chin J Geotech Eng* 6:52–58
- Feng P, Xu Y, Dai F (2021) Effects of dynamic strain rate on the energy dissipation and fragment characteristics of cross-fissured rocks. *Int J Rock Mech Min Sci* 138:104600. <https://doi.org/10.1016/j.ijrmms.2020.104600>
- Freire-Lista DM, Fort R, Varas-Muriel MJ (2016) Thermal stress-induced microcracking in building granite. *Eng Geol* 206:83–93. <https://doi.org/10.1016/j.enggeo.2016.03.005>
- Gong F, Si X, Li X, Wang S (2019) Dynamic triaxial compression tests on sandstone at high strain rates and low confining pressures with split Hopkinson pressure bar. *Int J Rock Mech Min Sci* 113:211–219. <https://doi.org/10.1016/j.ijrmms.2018.12.005>
- Grote DL, Park SW, Zhou M (2001) Dynamic behavior of concrete at high strain rates and pressures: I. experimental characterization. *Int J Impact Eng* 25:869–886

- Guha Roy D, Singh TN (2016) Effect of heat treatment and layer orientation on the tensile strength of a crystalline rock under Brazilian test condition. *Rock Mech Rock Eng*. <https://doi.org/10.1007/s00603-015-0891-y>
- Hajpál M, Török Á (2004) Mineralogical and colour changes of quartz sandstones by heat. *Environ Geol* 46:311–322. <https://doi.org/10.1007/s00254-004-1034-z>
- Janio de Castro LimaParaguassú JAB (2004) Linear thermal expansion of granitic rocks: influence of apparent porosity, grain size and quartz content. *Bull Eng Geol Env* 63:215–220. <https://doi.org/10.1007/s10064-004-0233-x>
- Jin P, Hu Y, Shao J, Zhao G, Zhu X, Li C (2019) Influence of different thermal cycling treatments on the physical, mechanical and transport properties of granite. *Geothermics* 78:118–128. <https://doi.org/10.1016/j.geothermics.2018.12.008>
- Kumari WGP, Ranjith PG, Perera MSA, Chen BK, Abdulagatov IM (2017) Temperature-dependent mechanical behaviour of Australian Strathbogie granite with different cooling treatments. *Eng Geol* 229:31–44. <https://doi.org/10.1016/j.enggeo.2017.09.012>
- Lemaitre J (1984) How to use damage mechanics. *Nucl Eng Des* 80:233–245. [https://doi.org/10.1016/0029-5493\(84\)90169-9](https://doi.org/10.1016/0029-5493(84)90169-9)
- Li JC (2013) Wave propagation across non-linear rock joints based on time-domain recursive method. *Geophys J Int* 193:970–985. <https://doi.org/10.1093/gji/ggt020>
- Li T, Li Z, Zhao Y (2006) Consistency of pore structures between NMR and mercury intrusion method. *Nat Gas Ind* 10:57–59
- Li JC, Li HB, Zhao J (2015a) An improved equivalent viscoelastic medium method for wave propagation across layered rock masses. *Int J Rock Mech Min Sci* 73:62–69. <https://doi.org/10.1016/j.ijrmms.2014.10.008>
- Li JC, Liu TT, Li HB, Liu YQ, Liu B, Xia X (2015b) Shear Wave Propagation Across Filled Joints with the Effect of Interfacial Shear Strength. *Rock Mech Rock Eng* 48:1547–1557. <https://doi.org/10.1007/s00603-014-0662-1>
- Li JC, Li NN, Li HB, Zhao J (2017) An SHPB test study on wave propagation across rock masses with different contact area ratios of joint. *Int J Impact Eng* 105:109–116. <https://doi.org/10.1016/j.ijimpeng.2016.12.011>
- Li Z, Yin S, Yue N, Cheng F, Liu S, Kong Y, Sun Y, Wei Y (2018) Experimental study on the infrared thermal imaging of a coal fracture under the coupled effects of stress and gas. *J Nat Gas Ence Eng* 55:444–451
- Li JC, Rong LF, Li HB, Hong SN (2019) An SHPB test study on stress wave energy attenuation in jointed rock masses. *Rock Mech Rock Eng* 52:403–420. <https://doi.org/10.1007/s00603-018-1586-y>
- Li M, Wang D, Shao Z (2020) Experimental study on changes of pore structure and mechanical properties of sandstone after high-temperature treatment using nuclear magnetic resonance. *Eng Geol* 275:105739. <https://doi.org/10.1016/j.enggeo.2020.105739>
- Li Z-W, Long M-C, Feng X-T, Zhang Y-J (2021) Thermal damage effect on the thermal conductivity inhomogeneity of granite. *Int J Rock Mech Min Sci* 138:104583. <https://doi.org/10.1016/j.ijrmms.2020.104583>
- Liu S, Xu J (2013) Study on dynamic characteristics of marble under impact loading and high temperature. *Int J Rock Mech Min Sci* 62:51–58
- Mahanta B, Singh TN, Ranjith PG (2016) Influence of thermal treatment on mode I fracture toughness of certain Indian rocks. *Eng Geol* 210:103–114. <https://doi.org/10.1016/j.enggeo.2016.06.008>
- Malaga-Starzec K, Åkesson U, Lindqvist JE, Schouenborg B (2006) Microscopic and macroscopic characterization of the porosity of marble as a function of temperature and impregnation. *Constr Build Mater* 20:939–947. <https://doi.org/10.1016/j.conbuildmat.2005.06.016>
- Meng F, Zhai Y, Li Y, Zhao R, Li Y, Gao H (2021) Research on the effect of pore characteristics on the compressive properties of sandstone after freezing and thawing. *Eng Geol* 286:106088. <https://doi.org/10.1016/j.enggeo.2021.106088>
- Ming X, Ming X (2017) Experimental study on mechanical properties and thermal damage characteristics of sandstone under high-temperature environment. *Min Res Dev* 9:2424
- Morrow C, Lockner D, Moore D, Byerlee J (1981) Permeability of granite in a temperature gradient. *J Geophys Res Solid Earth* 86:3002–3008
- Peng K, Lv H, Zou Q, Wen Z, Zhang Y (2020) Evolutionary characteristics of mode-I fracture toughness and fracture energy in granite from different burial depths under high-temperature effect. *Eng Fract Mech* 239:107306
- Qi C, Qian Q (2003) Physical mechanism of dependence of material strength on strain rate for rock-like material. *Chin J Rock Mech Eng* 22:177–181
- Ranjith PG, Viete DR, Chen BJ, Perera MSA (2012) Transformation plasticity and the effect of temperature on the mechanical behaviour of Hawkesbury sandstone at atmospheric pressure. *Eng Geol* 151:120–127. <https://doi.org/10.1016/j.enggeo.2012.09.007>
- Rao GMN, Murthy CR (2001) Dual role of microcracks: toughening and degradation. *Can Geotech J* 38:427–440. <https://doi.org/10.1139/t00-105>
- Rathnaweera TD, Ranjith PG, Gu X, Perera MSA, Kumari WGP, Wanniarachchi WAM, Haque A, Li JC (2018) Experimental investigation of thermomechanical behaviour of clay-rich sandstone at extreme temperatures followed by cooling treatments. *Int J Rock Mech Min Sci* 107:208–223. <https://doi.org/10.1016/j.ijrmms.2018.04.048>
- Rijaniaina RN, Beaucour A-L, Hebert RL, Ledesert B (2016) High temperature behaviour of a wide petrographic range of siliceous and calcareous aggregates for concretes - ScienceDirect. *Constr Build Mater* 123:261–273
- Róański A, Róańska A, Sobótka M, Pachnicz M, Bukowska M (2021) Identification of changes in mechanical properties of sandstone subjected to high temperature: meso- and micro-scale testing and analysis. *Arch Civ Mech Eng* 21:1–22
- Shao S, Wasantha PLP, Ranjith PG, Chen BK (2014) Effect of cooling rate on the mechanical behavior of heated Strathbogie granite with different grain sizes. *Int J Rock Mech Min Sci* 70:381–387. <https://doi.org/10.1016/j.ijrmms.2014.04.003>
- Shen Y-J, Hou X, Yuan J-Q, Wang S-F, Zhao C-H (2020) Thermal cracking characteristics of high-temperature granite suffering from different cooling shocks. *Int J Fract* 225:153–168. <https://doi.org/10.1007/s10704-020-00470-2>
- Sippel J, Siegesmund S, Weiss T, Nitsch KH, Korzen M (2007) Decay of natural stones caused by fire damage. *Geol Soc Lond Sp Publ* 271:139–151
- Sirdesai NN, Mahanta B, Ranjith PG, Singh TN (2019) Effects of thermal treatment on physico-morphological properties of Indian fine-grained sandstone. *Bull Eng Geol Environ* 78:883–897
- Sukontasukkul P, Nimityongskul P, Mindess S (2004) Effect of loading rate on damage of concrete. *Cem Concr Res* 34:2127–2134
- Tao M, Xue YA, Jm A, Yang YA, Wen LA, Jing ZA, Li EC (2020) Evolution of permeability and microscopic pore structure of sandstone and its weakening mechanism under coupled thermo-hydro-mechanical environment subjected to real-time high temperature. *Eng Geol* 280:105955
- Tian WL, Yang SQ, Huang YH (2018) Macro and micro mechanics behavior of granite after heat treatment by cluster model in particle flow code. *Acta Mech Sin* 34:1–12
- Wang Z, Li Y, Wang JG (2007) A damage-softening statistical constitutive model considering rock residual strength. *Comput Geosci* 33:1–9. <https://doi.org/10.1016/j.cageo.2006.02.011>

- Wang T, Yang C, Chen J, Daemen J (2018) Geomechanical investigation of roof failure of China's first gas storage salt cavern. *Eng Geol* 243:59–69
- Wong LNY, Zhang Y, Wu Z (2020) Rock strengthening or weakening upon heating in the mild temperature range? *Eng Geol* 272:105619. <https://doi.org/10.1016/j.enggeo.2020.105619>
- Xie H, Zhu J, Zhou T, Zhang K, Zhou C (2020) Conceptualization and preliminary study of engineering disturbed rock dynamics. *Geomech Geophys Geo-Energy and Geo-Resour* 6:34. <https://doi.org/10.1007/s40948-020-00157-x>
- Xu J, Kang Y, Hu Y, Liu F, Wang Z, Wang X (2021) Effects of hydrothermal treatment on dynamic properties of granite containing single fissure subject to impact loading. *Geomech Geophys Geo-Energy and Geo-Resour* 7:32. <https://doi.org/10.1007/s40948-021-00227-8>
- Yu M, Li S, Sun Q, Wang S (2021) Influence of grain size on the strain-rate-dependent dynamic response of sandstones. *Geomech Geophys Geo-Energy and Geo-Resour* 7:74. <https://doi.org/10.1007/s40948-021-00273-2>
- Zhang W, Sun Q, Zhu Y, Guo W (2019) Experimental study on response characteristics of micro–macroscopic performance of red sandstone after high-temperature treatment. *J Therm Anal Calorim* 136:1935–1945
- Zhang F, Zhang Y, Yu Y, Hu D, Shao J (2020) Influence of cooling rate on thermal degradation of physical and mechanical properties of granite. *Int J Rock Mech Min Sci* 129:104285. <https://doi.org/10.1016/j.ijrmms.2020.104285>
- Zhou Z, Zhao and Zhihong (2016) Thermal influence on mechanical properties of granite: a microcracking perspective. *Rock Mech Rock Eng* 49:747–762
- Zhou Z, Cai X, Chen L, Cao W, Zhao Y, Xiong C (2017) Influence of cyclic wetting and drying on physical and dynamic compressive properties of sandstone. *Eng Geol* 220:1–12. <https://doi.org/10.1016/j.enggeo.2017.01.017>
- Zuo JP, Xie HP, Zhou HW, Peng SP (2010) SEM in situ investigation on thermal cracking behaviour of Pingdingshan sandstone at elevated temperatures. *Geophys J Int* 181:593–603

Publisher's Note Springer Nature remains neutral with regard to jurisdictional claims in published maps and institutional affiliations.